Measurement of the LWFA Betatron source length by cross-correlations over images of granular random targets

Contact: n.carreira-lopes@imperial.ac.uk

N. C. Lopes[1,2], J.M. Cole[1], K. Poder[1], D. J. Chapman[3], J. C. Wood[1], S. Alatabi[1], M. E. Rutherford[3], D. Eakins[3], D. R. Symes[3], S. P. D. Mangles[1], Z. Najmudin[1]

[1] *The John Adams Institute for Accelerator Science, Imperial College London, SW7 2AZ, United Kingdom*

[2] *GoLP/Instituto de Plasmas e Fusão Nuclear, Instituto Superior Técnico, U.L., Lisboa 1049-001, Portugal*

[3] *Institute of Shock Physics, Imperial College London, SW7 2BW, United Kingdom*

[4] *Central Laser Facility, Rutherford Appleton Laboratory, Didcot OX11 0QX, UK*

Abstract

The blurring of images of a random granular target made with betatron radiation from a Laser Wakefield Accelerator (LWFA) was measured at different distances from the beam axis by using autocorrelations of the images. These measurements allowed an estimation of the evolution of the betatron emission length as a function of the density and length of the plasma accelerator.

1 Introduction

Betatron radiation is produced in Laser Wakefield Accelerators (LWFAs) [1, 2] resulting in high-quality broadband x-ray beams [3] that have been used to produce high-quality images of biological samples [4] as well as highly dynamic objects such as shocks in solids using their ultra-fast duration. It is the small source size of this radiation that allows its use for phase-contrast imaging [7, 8] and in high-resolution lenseless imaging for photon energies above 20 keV.

Along the plasma accelerator, the yield of the betatron emission is expected to scale with γ_e^2 (where γ_e the relativistic parameter of the electrons) [3]. Therefore we may expect that the betatron emission is mainly localised in the accelerator regions were the electrons reach maximum energies (for small variations of the electron beam charge along the accelerator). Therefore, even if the emission diameter remains of micron size, the emission extends to at least a few millimetres along the laser propagation axis which may result in increasing blurring with increasing distance from the beam axis.

In the context of a compact betatron imaging beamline, the x-ray source length is therefore an important parameter since it limits the useful diameter of the beam for imaging. We can see from the simplified setup geometry presented in figure 1 that the apparent x-ray source size, as a function of the distance to axis $R \approx \theta(d_1 + d_2)$ is given by

$$\phi_d \approx l_\beta \frac{R}{d_1 + d_2} \frac{d_2}{d_1}, \tag{1}$$

where l_β is the betatron source length, and d_1 and d_2 are the distances from source to sample and sample to detector respectively. The apparent source size for each detector region is the resolution limit that can be obtained for imaging in that region and ideally should not be larger that the detector pixel size or detector point-spread-function to avoid loss of resolution.

By mapping the image blurring as a function of the radius to axis, equation 1 can be used to find the x-ray emission length. Here we use x-ray phase-contrast images of sand paper (granular silicate dust, randomly displaced in a compacted cellulose fibre support), to measure the blurring (ϕ_d in equation 1) as a function of the distance to the x-ray beam axis. The local blurring is measured by autocorrelating small local samples of the images. When off-axis, the autocorrelation normally typically resembles a bivariate gaussian distribution with the longer axis pointing to the beam axis. The length of the longer axis is related to the blurring and is used in equation 1 to retrieve the betatron emission length. In this way, it is possible to measure the image resolution in

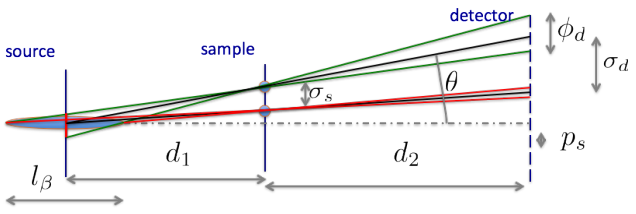

Figure 1: Simplified geometry of an imaging beam line showing the effect of the betatron source length on the off-axis image resolution.

the entire field of view in a single shot. It is also possible with a limited number of shots to optimise the source parameters (gas pressure and length) for imaging.

2 Experiment

The experiment was performed at a compact betatron beamline temporarily installed at the Astra-Gemini target area for imaging laser driven shocks in solids. The betatron x-ray beam was produced by a self-injected electron beam accelerated in a plasma wakefield driven by one of the Astra-Gemini laser beams (≈10 J, ≈45 fs, ≈800 nm, f/40, 1/20 Hz) in a gas cell of variable length, filled with helium to a given pressure with 1% precision immediately before each laser shot. The random target was placed at a fixed distance $d_1 = 0.925$ m and the detector was a distance $d_2 = 2.775$ m from the target, reducing equation 1 to $\phi_d \approx 0.81\, l_\beta\, R$ (all units in m). Several images of the random granular target were obtained for different values of pressure and gas cell length in order to study the evolution of the betatron source length with these two parameters (these are the parameters easily available to tune the resolution versus brightness of a betatron x-ray imaging beamline).

The x-ray detector used in this experiment was a commercial indirect detection x-ray camera [5, 6]. The camera uses a structured scintillator that has its fluorescence light transported to the camera CCD chip by a high resolution fibre bundle. The imperfections of this detector can be almost completely corrected with a suitable flat-field that needs to be previously obtained with no target in the beamline. The image quality is then enhanced by correcting the grey values of exceptionally hot pixels (caused by a low number of hot photons likely produced by bremsstrahlung radiation of electrons hitting the beamline elements or by rare high-energy betatron photons) and exceptionally cold pixels (caused mainly by imperfections in the flat field correction).

3 X-ray imaging blur mapping

A typical image of the granular target used in this experiment can be seen in figure 2-a). In these images the darker squares on the corners are filters of different elements used to infer the critical energy of the betatron beam. Samples of the image with a radius of 120 pixels are taken at regular spacing of 100 pixels. Larger radii break the assumption that the apparent source size is constant across the sample, smaller radii reduce the precision of the autocorrelation. In figure 2-b) the central region of the autocorrelation samples (where the signal is strongest) are superimposed on the original x-ray image. The central regions of the autocorrelations are plotted in detail in figure 2-c). The autocorrelation peaks are approximately gaussian with the larger axis directed towards the centre of the x-ray beam, and the length of

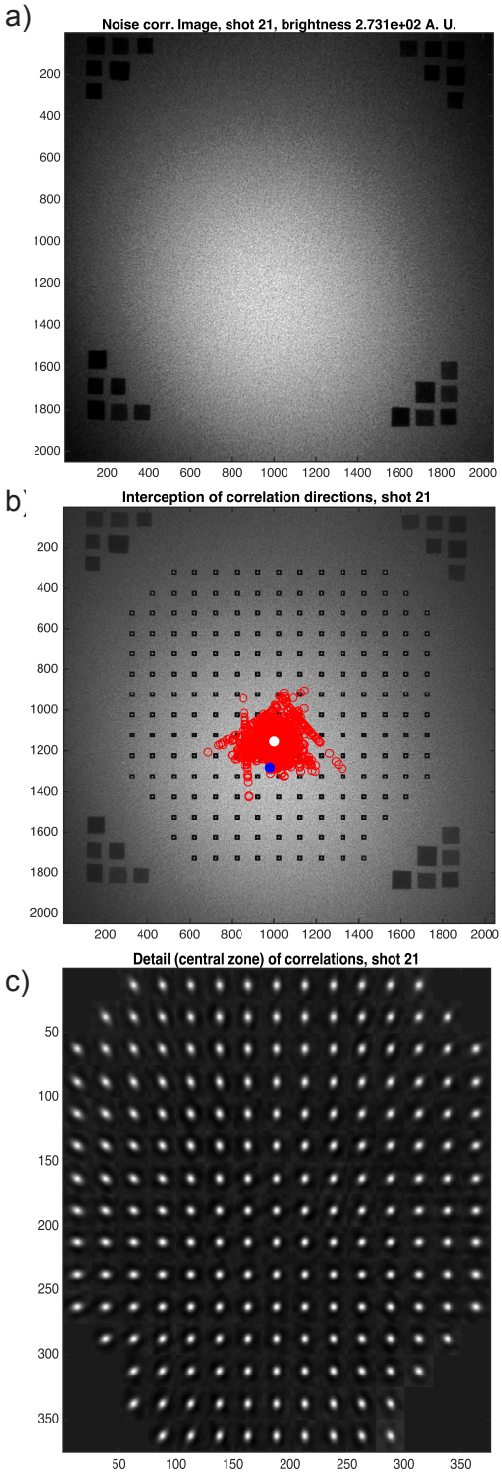

Figure 2: a) Typical image of the granular target (L = 20 mm, P = 70 mbar), b) Image with the central parts of the autocorrelations superimposed on the sampling centres, with interceptions of angles (red), centre of the beam (white) and betatron beam centre of gravity (blue), c) Composite image made with the central parts of the autocorrelations.

the axis increases with distance to the beam axis as expected. In figure 2-b) the interceptions of the directions of the long axes of the autocorrelations are plotted as red circles (for interceptions with angle differences $> 20°$), and their average position (white circle) taken as the beam axis to account for calculating the distance to axis R of the different samples. Also in figure 2-b) the blue circle represents the position of the centre of gravity of the beam, calculated using the 25% brightest pixels to avoid the impact of the filters in the image corners.

The autocorrelations are approximately symmetric. By fitting a two-dimensional bivariate gaussian function to each autocorrelation it is possible to map the blurring along the image and to infer the x-ray emission length. For each autocorrelation, besides the angle that points to centre of the beam, it is possible to extract the long and short axes of the gaussian σ_{long} and σ_{short}. σ_{short} is approximately constant not only throughout an image, but also for images with different accelerator parameters (pressure and length) which produce x-ray beams of reasonable quality. This behaviour can be explained if σ_{short} is the effective source size resulting from the convolution of the source diameter by the detector point spread function (PSF_d), where the latter is expected to dominate.

The obtained images $I(x, y)$ are a local convolution of the speckle pattern $I_0(x, y)$ and a point spread function $P(x, y)$, or

$$I = I_0 * P. \tag{2}$$

We measure the autocorrelation $A = I * I$ of I, which Fourier transforms as $\tilde{A} = \tilde{I_0^2}\tilde{P^2}$. If the granular target is isotropic and approximately periodic with grain size $\sim \sigma$, the Fourier transform of $I_0 * I_0$ is $\tilde{I_0^2}$, where $\tilde{I_0} \propto e^{-\sigma^2 k^2/2}$ with $k^2 = k_x^2 + k_y^2$. If the PSF P is assumed to be a symmetric gaussian convolved uniformly by the projected length of the plasma in the y direction, (ϕ_d in figure 1), then

$$P(x, y) \propto e^{-(x^2+y^2)/2\sigma_s^2} * \text{rect}_{\phi_d}(y) \tag{3}$$

where rect_{ϕ_d} is 1 for $-\phi_d/2 < y < \phi_d/2$ and 0 otherwise, and σ_s is the x-ray source size. The Fourier transformed autocorrelation becomes

$$\tilde{A} = e^{-(\sigma^2+\sigma_s^2)k_x^2} e^{-\sigma^2 k_y^2} \,\text{sinc}^2(k_y\phi_d/2) \tag{4}$$

which, assuming $\sigma_s \ll \sigma$, inverse Fourier transforms to

$$A(x, y) = e^{-(x^2+y^2)/\sigma^2} * \text{triangle}_{\phi_d}(y) \tag{5}$$

where $\text{triangle}_{\phi_d}(y)$ is the autoconvolution of $\text{rect}_{\phi_d}(y)$ with full width half maximum ϕ_d. To extract ϕ_d from the autocorrelation $A(x, y)$ one can show that the best-fit gaussian to $A(x, y)$ satisfies

$$\phi_d = \sqrt{1.3(\sigma_{\text{long}}^2 - \sigma_{\text{short}}^2)} \pm 2\% \tag{6}$$

from which l_β can be extracted using equation 1.

4 Experimental results and discussion

Images of the same granular target were taken for a range of different pressures and gas target lengths. The images were processed as described above resulting in an estimated source emission length for each autocorrelation. The mean values of the source lengths $\overline{l_\beta}$ are plotted in figure 3 a). In figure 3 b) we present the obtained x-ray yield averaged over the image in arbitrary units (here the actual CCD average count number divided by 1000) for a fixed beamline configuration.

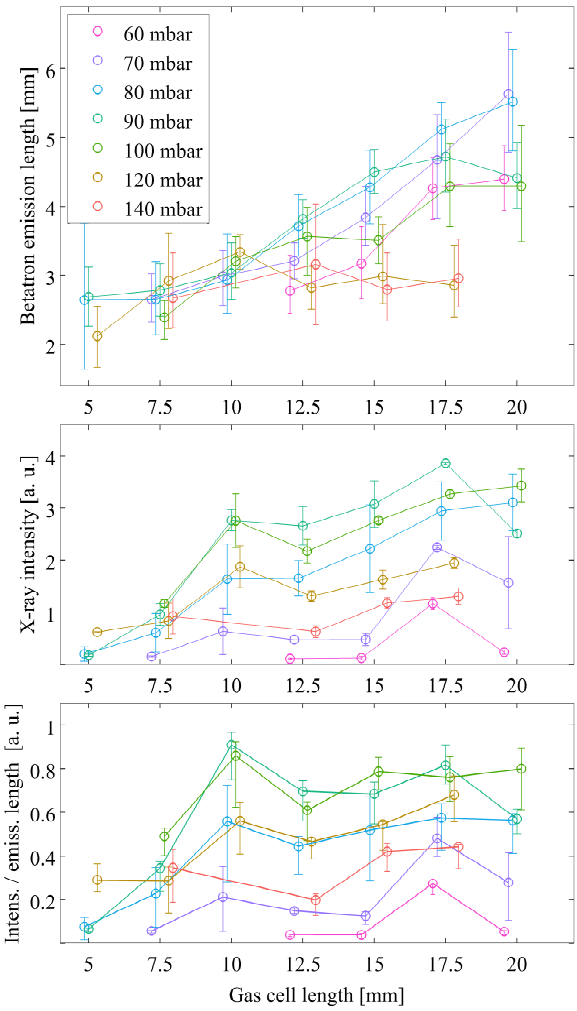

Figure 3: a) Betatron emission lengths, b) x-ray intensity and c) the ratio of the intensity to the emission length, as a function of gas cell length for several pressures. The gas cell lengths used were 5 mm, 7.5 mm, 10 mm, 12.5 mm, 15 mm, 17.5 mm and 20 mm. The data points for different pressures are slightly displaced in x for clarity.

In figure 3 a) and b) each data point results from the averaging of 1 - 4 shots. The error bars in figure 3-b) represent the variation of the x-ray yield between shots with the same parameters. In figure 3-c) we display the ratio (x-ray yield/emission length), a possible figure of merit for a compact LWFA imaging beamline.

Since the betatron radiation yield scales with γ_e^2, we can expect that in general the x-ray emission is produced in a limited length where the accelerated electrons reach their highest energies. Therefore the increase of the cell length never produces an equal increase in the emission length, although it increases monotonically for low and moderate pressures as seen in figure 3-a). The electron beam, here produced by self-injection into the accelerating wakefield structure, starts to reliably attain energies above 1 GeV for gas pressures above 60 mbar. However the x-ray yield (also proportional to the electron charge and emission length) only becomes adequate for imaging for slightly higher pressures (70 to 100 mbar) likely due to the increase in the beam charge and wiggler parameter [5].

For the highest pressures (> 100 mbar) the x-ray yield is reduced. The higher injected charge is likely not enough to compensate the lower energy attained by the electron beam, and also the smaller region over which high energies are maintained.

Taking the ratio (x-ray yield/emission length) as the quantity to maximise, we can see from figure 3-c) that the optimum parameters are a pressure of 90 mbar for a cell length of 10 mm. Here the x-ray yield is close to the maximum (corresponding to ≈ 3000 counts on a 16 bit CCD with no gain), and the blurring at 1 cm radius given by equation 1 is approximately 25 μm, approximately the size of 2 detector pixels.

5 Conclusion

The betatron emission length and its consequences for image quality was measured using the autocorrelation of phase-contrast images of a granular target. This single-shot diagnostic allowed the optimisation of the beamline parameters in order to attain an adequate compromise between x-ray yield and image resolution. For the beamline configuration (parameters d_1 and d_2) it is possible to identify the parameters of the electron and x-ray source (pressure, length) that maximise the ratio (x-ray yield/emission length). For the optimal source parameters the maximum blurring corresponds to approximately 2 pixels, which is close to the size of the average detector PSF. Therefore, for these parameters, the source length does not have a significant impact on the obtainable image resolution.

References

[1] Esarey, E., Shadwick, B. A., Catravas, P. & Leemans, W. P. Synchrotron radiation from electron beams in plasma-focusing channels. *Phys. Rev. E*, **65,** 056505 (2002).

[2] Rousse, A. *et al.* Production of a keV x-ray beam from synchrotron radiation in relativistic laser-plasma interaction. *Phys. Rev. Lett.*, **93,** 135005 (2004).

[3] Kneip, S. *et al.* Bright spatially coherent synchrotron x-rays from a table-top source. *Nature Phys.*, **6,** 980–983 (2010).

[4] J. M. Cole, J. C. Wood, N. C. Lopes, et al., Laser-wakefield accelerators as hard x-ray sources for 3D medical imaging of human bone, Scientific Reports 5, 13244 (2015)

[5] J. C. Wood, K. Poder, N. C. Lopes, et al., Enhanced Betatron Radiation from a Laser Wakefield Accelerator in a Long Focal Length Geometry To be published in this RAL report (2017)

[6] J. C. Wood, S. P. D. Mangles, Z. Najmudin, et al., Calibration of the CLF Andor iKon Indirect Detection X-ray Camera To be published in this RAL report (2017)

[7] Kneip, S. *et al.* X-ray phase contrast imaging of biological specimens with femtosecond pulses of betatron radiation from a compact laser plasma wakefield accelerator. *Appl. Phys. Lett.*, **99,** 093701 (2011).

[8] Fourmaux, S. *et al.* Single shot phase contrast imaging using laser-produced betatron x-ray beams. *Opt. Lett.*, **36,** 2426–2428 (2011).